Optimal checkerboard selection for structured light system calibration

William Lohry, Ying Xu, and Song Zhang*

Department of Mechanical Engineering, Iowa State University, Ames, IA, USA 50011.

ABSTRACT

Structured light system calibration has been widely studied over the decades, and a variety of calibration approaches have been proposed. Among these methods, the flexible method using flat checkerboard is widely adopted. However, there is a lack of studies on selecting the optimal checker size for high accuracy calibration, whilst it is vital to understanding this factor. This paper presents a systematic study on how the checker size affects the calibration accuracy for a structured light system, and provides a general guideline to select the optimal size. For this initial study, 7 different checker sizes are selected, and experiments demonstrated that the system achieved the best calibration accuracy within a certain range of checker size.

Keywords: Calibration; structured light; phase shifting; checker size; three dimensional; scanner.

1. INTRODUCTION

For any three-dimensional (3D) shape measurement system, its calibration accuracy is one of the key determinant factors for final measurement accuracy. Thus, improving the calibration accuracy of a structured light system is vital for high accuracy measurement.

Structured light system calibration has been widely studied over the decades,[1–9] and a variety of calibration approaches have been proposed. Among these methods, the flexible method, proposed by Zhang,[10] that uses a flat checkerboard is widely utilized to calibrate a camera. For Zhang's method, the intrinsic and extrinsic parameters of the camera are estimated from the checkerboard images at difference poses. Because the optics of a projection system, especially those with a digital micromirror device (DMD), is similar to that of a camera system in that both systems contain a lens and an imaging sensor. In fact, the projector can be treated as an inverse of a camera (i.e., instead of capturing images, it projects images), the calibration of a projection system should be theoretically the same as that of a camera. However, the difficulty remains because the projector is not as flexible as a camera since it cannot capture images. Zhang and Huang made it possible by allowing the projector "capture" images like a camera.[11] In this method, by using a phase-shifting technique, the one-to-one mapping between the projector pixel and the camera pixel is established, therefore, the camera image can be mapped onto the projector image. By this means, it seems the projector can "capture" images like a camera. Thus, the calibration of a structured light system becomes a well-studied calibration of a stereo system. Because the projector and camera calibration are independent (to some extent), the calibration accuracy is significantly improved, and the calibration speed is drastically increased. Following this work, a number of calibration techniques have been proposed,[12–15] but they are essentially the same in that all of these techniques are to establish the correspondences between the projector and the camera point by point. Once the system is calibrated, the *xyz* coordinates can be computed from the "absolute" phase.

Even though the flat checkerboard has been widely implemented for structured light system calibration, there is a lack of studies on selecting the optimal checker size for high accuracy calibration, whilst it is vital to understanding this factor. In this research, we will systematically study how the checker size affects the measurement accuracy, and provide a general guideline to select the optimal size for high accuracy system calibration.

In particular, we will use the approach proposed by Zhang and Huang[11] to generate the projector images and follow its similar calibration procedures. The key to this method is to accurately map the images acquired by the camera to those of the projector. In other words, the projector images are generated by establishing the one-to-one mapping between these two sensors. The mapping is established through absolute phase while the absolute phase is obtained by projecting an additional "centerline" images and detecting the center of lines. Our experiments found that the precision of detecting the centerlines will affect the accuracy of the projector image generation, that can be verified by projecting the projector images onto the physical object and find the differences. To alleviate this problem, Li et al. used an optimal wavelength

*song@iastate.edu; phone 1 515 294 0723; fax 1 515 294 3261; www.vrac.iastate.edu/~song.

selection approach.[13] For this approach, because only three wavelengths are used, the fringe noises play a significant role for accurate projector image generation because the longest-wavelength fringe images must be used.

To further alleviate the problem induced the centerline detection used in Zhang and Huang's method and the method adopted by Li et al.,[13] we use a digital multiple-wavelength phase-shifting method for our study.[16] The advantage of this digital multiple-wavelength algorithm is that the noise level is comparable to that of a single-wavelength phase-shifting technique while the absolute phase is obtained pointwise with sub pixel accuracy. Therefore, it significantly reduced the mapping error caused by the centerline detection or the noise by optimal wavelength selection approach.

As addressed previously, once the camera and the projector images are obtained, the calibration of a structured light system essentially becomes that of a well-studied stereo system. However, because the camera and the projector are both digital devices that sample the physical checkerboard at certain spatial resolution, the digital effect should play a big role on calibration accuracy if a flat checkerboard calibration method is adopted. The corner detection accuracy relies heavily on the size of the checkerboard, thereby the size of checker squares significantly affects the accuracy of the estimated parameters. As a result, the calibration accuracy is influenced by the selection of the checker square size. Intuitively, this is obvious, if there are too few pixels in one checker square, it is very difficult to find the corners accurately because each pixel represents more percentage of the checker. On the other hand, if the checkers are too large, there are not sufficient corners to use to know how the image is distorted, thus it is difficult to obtain the lens distortion error accurately. Therefore, the checkerboard selection is essential to calibrating the structured light system accurately. Experimental results will be presented to demonstrate the optimal range of checker size to use in order to achieve high accuracy.

Section 2 introduces the principle of the system. Section 3 shows some experimental results, and Sec. 4 summarizes this paper.

2. PRINCIPLE

2.1 Digital multiple-wavelength phase-shifting algorithm

Phase-shifting algorithms are widely adopted in optical metrology because of their speed and non-surface-contact nature.[17] Over the years, a variety of phase shifting algorithms have been proposed, including three-step, four-step, and five-step algorithms. To avoid the problems caused by a conventional spatial phase unwrapping algorithm, multiple-wavelength phase-shifting algorithms have been proposed.[18–22] For these techniques, the minimum number of three frequencies are required,[22] where at least 9 fringe images have to be used. Multiple-wavelength methods certainly will reduce the measurement speed because more fringe images are required. However, because the calibration only needs to be performed once, the speed is not a big factor to be considered in this study. To alleviate the problems induced the centerline detection used in Zhang and Huang's method, and the three wavelength method adopted by Li et al,[13] we use a digital multiple-wavelength phase-shifting algorithm.[16]

For a three-step phase-shifting algorithm, only three images are required to compute the phase. In particular, three fringe images of a three-step phase-shifting algorithm with a phase shift of $2\pi/3$ can be represented as

$$I_k(x,y) = I'(x,y) + I''(x,y)\cos\left[\frac{2\pi h(x,y)}{\lambda} + \frac{2k\pi}{3}\right], \tag{1}$$

where $k = 0, 1, 2$, $I'(x,y)$ is the average intensity, $I''(x,y)$ the intensity modulation, and $h(x,y)$ is the spacial distance. The phase to be solved for is

$$\phi(x,y) = \frac{2\pi h(x,y)}{\lambda}. \tag{2}$$

In general, $\phi(x,y)$, ranges from $-\pi$ to $+\pi$ by direct calculation of a set of fringe images.[17] The real phase, $\Phi(x,y)$, should be continuous as a function of $\phi(x,y)$. To obtain the real phase, a conventional phase unwrapping algorithm can be adopted.[23] The phase unwrapping process is essentially to find the integer number $m(x,y)$ for point (x,y) so that

$$\Phi(x,y) \quad = \quad 2\pi m(x,y) + \phi(x,y). \tag{3}$$

$\Phi(x,y)$ represents the true phase (or the unwrapped phase). If only a single fringe stripe is used, because $\phi(x,y) = \Phi(x,y)$ and $m(x,y) \equiv 0$, no phase unwrapping is necessary. In this research, we use the wavelengths as $\lambda_k = N\lambda_{k+1)}$, $k = 1,2,3,\cdots$.

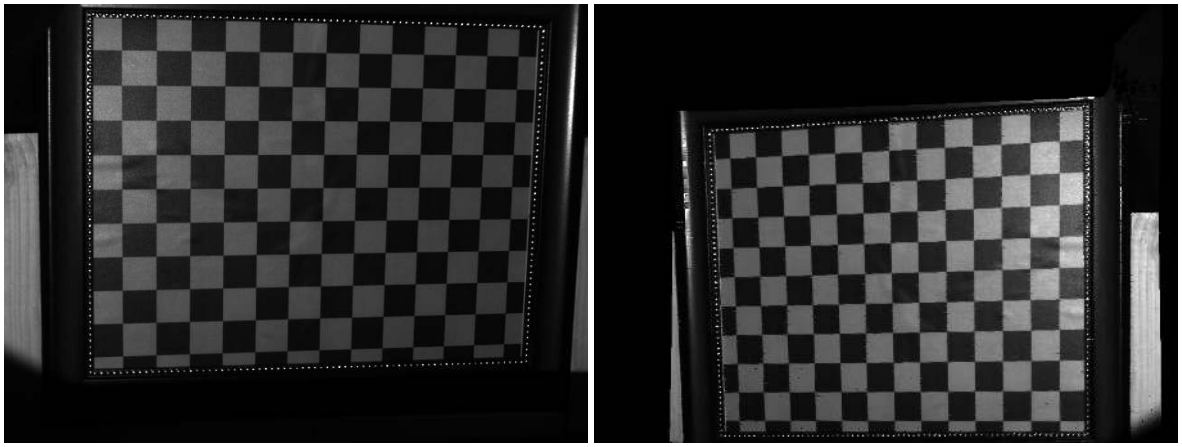

(a) (b)

Fig. 1. Calibration image pair for the projector image and the camera image. (a) The camera image; (b) The corresponding projector image.

Assume the projector has a resolution of $W \times H$ and the fringe stripes are vertical. If we choose $\lambda_1 = W$, there is no need for phase unwrapping because the single fringe covers the whole area. That is,

$$\Phi_1(x,y) = \phi_1(x,y). \tag{4}$$

Here, $\phi_1(x,y)$ represents the wrapped phase, and $\Phi_1(x,y)$ is the corresponding unwrapped phase.

Because $\lambda_k = \lambda_{k-1}/N$, we have $\Phi_k = N\Phi_{k-1}$. Combining with Eq.(3), we have

$$m_k(x,y) = \text{Round}\left[\frac{N\Phi_{k-1}(x,y)}{2\pi} - \frac{\phi_k(x,y)}{2\pi}\right], \tag{5}$$

and

$$\Phi_k(x,y) = 2\pi m_k(x,y) + \phi_k(x,y). \tag{6}$$

The multiple-wavelength phase shifting algorithm provides an absolute phase, so the correspondence between the phase line on the projector and the camera can be uniquely correlated and the one-to-one mapping can be established easily. The projector image creation based on the mapping will be addressed in the next section.

2.2 Projector image creation

Because the absolute phase is known by utilizing a multiple-wavelength phase-shifting algorithm, the one-to-one mapping between the camera image and the projector can be established by projecting horizontal fringe stripes and vertical stripes. For the horizontal fringe stripes, each point (p) on the camera image corresponds to one horizontal line (l_h) on the projector image; for the vertical stripes, the same point (p) on the camera image corresponds to one vertical line (l_v)on the projector image; and the intersection between line l_h and l_v is a unique point, which is the corresponding projector image point for point p. If this operation is performed point by point, the projector image can be generated by taking the intensity information of the camera image for the corresponding point. Figure 1 shows an example of the corresponding images between the projector image and the camera image.

2.3 System parameter estimation

Because the projector becomes a camera, the model of a projector is the same as that of a camera. The camera model used in this research is described thoroughly in Reference[10] by Zhang. For this model, the camera is described as a pinhole model, with intrinsic parameters including focal length, principle point, pixel skew factor, and pixel size; and extrinsic parameters including rotation and translation from the world coordinate system to the camera coordinate system.[11] For

(a) (b)

Fig. 2. (a) Photograph of the 3D shape measurement system; (b) Photograph the universal mounting frame to hold calibration board.

a linear model, the relationship between the world coordinate (x^w, y^w, z^w) and the camera image coordinate (u, v) can be written as

$$s\{u, v, 1\}^T = A[\ R, \quad t\ ]\{x^w, y^w, z^w, 1\}^T, \tag{7}$$

where s is a scale factor. $[R, t]$, called extrinsic parameters matrix, represents the rotation and the translation between world coordinate system and camera coordinate system. A is camera intrinsic parameters matrix and can be expressed as

$$A = \begin{bmatrix} \alpha & \gamma & u_0 \\ 0 & \beta & v_0 \\ 0 & 0 & 1 \end{bmatrix},$$

here (u_0, v_0) is the coordinate of principle point, α and β are focal lengthes along u and v axes of the image plane, and γ is the parameter that describes the skewness of two image axes. Eq. (7) represents the linear model of the camera. For this research, we found that the linear model is not sufficient, thus nonlinear compensation is therefore implemented. In this research, we use the method described in Reference,[12] and only consider the nonlinear effect till 4th order radial distortion, and 2nd tangential distortion.[10] Our experiments showed that, this consideration is sufficient to achieve high accuracy measurement, which will be explained in Sec. 3.

3. EXPERIMENTS

3.1 Calibration system design

The structured light system include the Dell LED projector (M109S), The Imaging Source digital USB CCD camera (DMK 21BU04), and Computar M0814-MP (F1.4) Lens. The projector has a resolution of 858 $\times$ 600, with 10,000 hours usage life time. The brightness of the projector is 50 ANSI Lumens. The projection lens is F/2.0, f = 16.67 mm fixes lens. The projection distance is 23.6-94.5 inches. The DMD used in this projector is 0.45-inch Type Y chip. The camera resolution is 640 $\times$480, with a maximum frame rate of 60 frames/sec. The camera output 8 bit image at full resolution, the pixel size is 5.6 $\times$ 5.6 μm^2. Figure 2(a) shows the photograph of the system.

The calibration checkerboard is held by a universal mounting frame, that has six degree of freedom (DOF). As shown in Figure 2(b). This universal mounting frame allows us to position the checkerboard easily and accurately. The checkerboard picture is glued on a flat glass surface in a picture frame. The 6-DOF mounting frame has a sliding holder that can hold the picture frames.

3.2 Experimental procedures

For this research, we used a total of seven different checker sizes, with the dimension 6.23, 10.02, 15.99, 20.03, 23.94, 30.94, 34.98 mm squares. For each checker square size, 30 different poses are imaged. Once all these images are acquired, the intrinsic parameters of the camera and the projectors are estimated using the Matlab calibration ToolBox and set the

fifth distortion parameters as 0.[24] The extrinsic parameters are estimated based on the same pose image for different checkerboards. A typical calibration results is

$$A^c = \begin{bmatrix} 1473.14109 & 0 & 318.58100 \\ 0 & 1478.75600 & 296.50674 \\ 0 & 0 & 1 \end{bmatrix}, \quad (8)$$

$$R^c = \begin{bmatrix} 0.040603 & 0.998324 & -0.041242 \\ 0.997559 & -0.038156 & 0.058487 \\ 0.056815 & -0.043516 & -0.997436 \end{bmatrix}, \quad (9)$$

$$t^c = \{-122.170542, -134.481918, 838.150649\}^T, \quad (10)$$

$$D^c = [-0.09386, 0.00000, 0.00108, -0.00315, 0.00000]. \quad (11)$$

for the camera, here D^c is the distortion vector that is defined in .[24] Similarly, we can obtain projector calibration parameters

$$A^p = \begin{bmatrix} 1539.65117 & 0 & 396.04641 \\ 0 & 1661.69004 & 562.93291 \\ 0 & 0 & 1 \end{bmatrix}, \quad (12)$$

$$R^p = \begin{bmatrix} 0.039962 & 0.998776 & -0.029135 \\ 0.998749 & -0.040804 & -0.028901 \\ -0.030054 & -0.027944 & -0.999158 \end{bmatrix}, \quad (13)$$

$$t^p = \{-140.570514, -176.480294, 856.234265\}^T, \quad (14)$$

$$D^p = [0.15233, -0.59555, -0.00275, -0.00609, 0.00000]. \quad (15)$$

3.3 Error evaluations

With all these calibration parameters estimated from different checker size, a flat surface is then measured to compare the measure quality. The measured surface is fitted to an ideal flat plane function $ax+by+cz=1$. Once the plane is fitted, the measurement error can be estimated as follows:

Assume there are N number of measurement points, which can be fitted to a plane function

$$ax+by+cz=1.$$

For all these given points, we have

$$AX = b_0$$

where A is a $M \times 3$ matrix whose entries are,

$$A_{i0} = x_i;$$

$$A_{i1} = y_i;$$

$$A_{i2} = z_i;$$

$X = \{a,b,c\}^T$, b_0 is a $M \times 1$ vector, whose entries are all 1. The least square solution is,

$$X = (A^T A)^{-1} A^T b_0.$$

After we obtained the ideal plane, we can get the error map, which is for any given measured point $\mathbf{p}(\mathbf{x},\mathbf{y},\mathbf{z})$, which is

$$d = |\mathbf{n} \cdot (\mathbf{p} - \mathbf{p_0})|$$

where $\mathbf{p}$ the measurement point, $\mathbf{p_0}$ is an arbitrary point on the ideal plane, and $n = (a,b,c)/\sqrt{a^2+b^2+c^2}$ is the normalized normal of the ideal plane (As illustrated in Figure 3).

Table 1 summarizes the errors for these checker sizes, and Fig. 4 shows the correlation between the calibration error and the checker square size. It is obvious that if the checker size is too small, the calibration cannot be performed accurately.

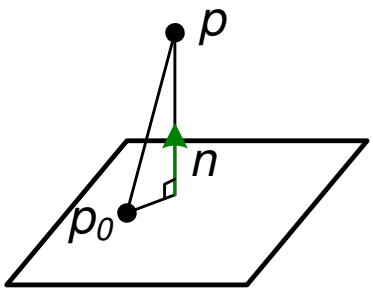

Fig. 3. Distance from a point to a plane

Table 1. System parameters estimated from different checker boards

Checker Size (mm)	6.23	10.02	15.99	20.03	23.94	30.94	34.98
Camera pixels per checker square	10.79	17.36	25.98	34.71	41.48	52.00	60.61
Projector pixel per checker square	11.83	19.03	28.47	38.04	45.47	57.00	66.43
RMS error (mm)	7.92	1.35	1.19	1.19	1.19	1.35	1.57

This is because the number of pixels per checker square is very too few, the corner detection error will be dominant. For example, when the checker size reduces to 6.23 mm, with only about 11 pixels for the camera image and 12 pixels for the projector image, the RMS error is 7.92 mm. From this experiment we can draw the conclusion that in order to do good calibration, there must be enough camera pixels to represent one checker squares.

When the checker size increases, the calibration error decreases. This is understandable, because the corner detection error relatively decreases. However, when the checker size increases beyond certain value, the calibration error increases again. This is mostly caused by the number of points for parameter estimation becoming less and less. The lens distortions are more and more difficult to be accurately estimated because of the lack of points are used.

The most accurate calibration happens if the checker square size is around 25 mm, when the number of pixels per checker square is around 35 for camera and 38 for the projector. This experiment demonstrated that indeed there is an optimal size of checker board to use for a structured system calibration. For our system, the size is around 25 mm.

4. CONCLUSIONS AND FUTURE WORKS

This paper has presented a study on how to choose the optimal checker size for accurate structured light system calibration. In this study, we will use the approach proposed by Zhang and Huang to generate the projector image and to calibrate the structured light system. For this method, with the assistance of the camera, the projector can "capture" images like a camera point by point by adopting a digital multiple-wavelength phase-shifting method. Due to the digital effect of the camera and the projector, the corner detection accuracy of the software algorithm, the size of checker squares significantly affects the accuracy of the estimated parameters.We have systematically studied how the checker size affects the measurement accuracy, and have provided a general guideline to select the optimum size for high accuracy system calibration. Experiments have verified the existence of the optimal checker square size. In the future, we will perform more studies to narrow down the checker square size difference and to find the systematic correlation between the calibration error and the checker size.

ACKNOWLEDGEMENT

This work was supported by the Startup Funds of Dr. Song Zhang at Iowa State University, and partially sponsored by ISU Honor's Program.

REFERENCES

[1] Legarda-Sáenz, R., Bothe, T., and Jüptner, W. P., "Accurate procedure for the calibration of a structured light system," *Opt. Eng.* **43**(2), pp. 464–471, 2004.

[2] Cuevas, F. J., Servin, M., and Rodriguez-Vera, R., "Depth object recovery using radial basis functions," *Opt. Commun.* **163**(4), pp. 270–277, 1999.

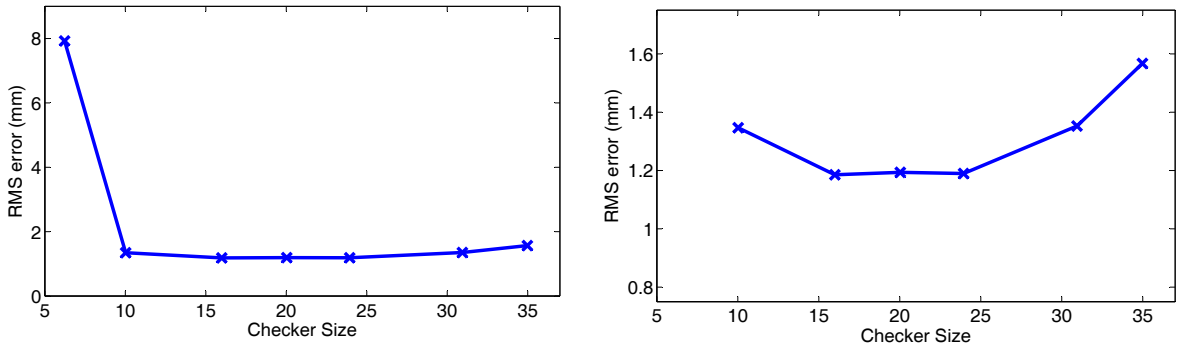

(a) (b)

Fig. 4. RMS Error over the checker size. (a) All 7 checker sizes; (b) 2-6 checker sizes.

[3] Cuevas, F. J., Servin, M., Stavroudis, O. N., and Rodriguez-Vera, R., "Multi-layer neural networks applied to phase and depth recovery from fringe patterns," *Opt. Commun.* **181**(4), pp. 239–259, 2000.

[4] Hu, Q., Huang, P. S., Fu, Q., , and Chiang, F. P., "Calibration of a 3-d shape measurement system," *Opt. Eng.* **42**(2), pp. 487–493, 2003.

[5] Fraser, C. S., "Photogrammetric camera component calibration: A review of analytical techniques," in *Calibration and Orientation of Camera in Computer Vision*, Gruen, A. and Huang, T. S., eds., pp. 95–136, Springer-Verlag, (Berlin Heidelberg), 2001.

[6] Gruen, A. and Beyer, H. A., "System calibration through self-calibration," in *Calibration and Orientation of Camera in Computer Vision*, Gruen, A. and Huang, T. S., eds., pp. 163–194, Springer-Verlag, (Berlin Heidelberg), 2001.

[7] Heikkilä, J., "Geometric camera calibration using circular control," *IEEE Trans. Pattern Anal. Mach. Intell.* **PAMI-22**(10), pp. 1066–1077, 2000.

[8] Pedersini, F., Sarti, A., and Tubaro, S., "Accurate and simple geometric calibration of multi-camera systems," *Signal Process* **77**(3), pp. 309–334, 1999.

[9] Gennery, D. B., "Least-square camera calibration including lens distortion and automatic editing of calibration points," in *Calibration and Orientation of Camera in Computer Vision*, Gruen, A. and Huang, T. S., eds., pp. 123–136, Springer-Verlag, (Berlin Heidelberg), 2001.

[10] Zhang, Z., "A flexible new technique for camera calibration," *IEEE Trans. Pattern Anal. Mach. Intell.* **22**(11), pp. 1330–1334, 2000.

[11] Zhang, S. and Huang, P. S., "Novel method for structured light system calibration," *Opt. Eng.* **45**, p. 083601, 2006.

[12] Huang, P. and Han, X., "On improving the accuracy of structured light systems," in *Proc. SPIE*, **6382**, p. 63820H, 2006.

[13] Li, Z., Shi, Y., Wang, C., and Wang, Y., "Accurate calibration method for a structured light system," *Opt. Eng.* **47**(5), p. 053604, 2008.

[14] Yang, R., Cheng, S., and Chen, Y., "Flexible and accurate implementation of a binocular structured light system," *Opt. Lasers Eng.* **46**(5), pp. 373–379, 2008.

[15] Gao, W., Wang, L., and Hu, Z., "Flexible method for structured light system calibration," *Opt. Eng.* **47**(8), p. 083602, 2008.

[16] Zhang, S., "Digital multiple-wavelength phase-shifting algorithm," in *Proc. SPIE*, 2009.

[17] Malacara, D., ed., *Optical Shop Testing*, John Wiley and Sons, New York, 3rd ed., 2007.

[18] Cheng, Y.-Y. and Wyant, J. C., "Multiple-wavelength phase shifting interferometry," *Appl. Opt.* **24**, pp. 804–807, 1985.

[19] Mehta, D. S., Dubey, S. K., Shakher, C., and Takeda, M., "Two-wavelength talbot effect and its application for three-dimensional step-height measurement," *Appl. Opt.* **45**, pp. 7602–7609, 2006.

[20] Warnasooriya, N. and Kim, M. K., "Led-based multi-wavelength phase imaging interference microscopy," *Opt. Express* **15**, pp. 9239–9247, 2007.

[21] Towers, D. P., Jones, J. D. C., and Towers, C. E., "Optimum frequency selection in multi-frequency interferometry,"

Opt. Lett. **28**, pp. 1–3, 2003.

[22] Towers, C. E., Towers, D. P., and Jones, J. D. C., "Absolute fringe order calculation using optimised multi-frequency selection in full-field profilometry," *Opt. Laser Eng.* **43**, pp. 788–800, 2005.

[23] Ghiglia, D. C. and Pritt, M. D., *Two-Dimensional Phase Unwrapping: Theory, Algorithms, and Software*, John Wiley and Sons, Inc, 1998.

[24] Bouguet, J.-Y., "Camera calibration toolbox for matlab." Online available at: http://www.vision.caltech.edu/bouguetj/calib_doc.